Contents lists available at ScienceDirect

Geochimica et Cosmochimica Acta

journal homepage: www.elsevier.com/locate/gca

Mapping the redox state of the young Solar System using ytterbium valence state

Tahar Hammouda [a,*], Paul Frossard [a,b], Maud Boyet [a], Audrey Bouvier [c], Matthew Newville [d], Antonio Lanzirotti [d]

[a] Université Clermont Auvergne, CNRS, IRD, OPGC, Laboratoire Magmas et Volcans, F-63000 Clermont-Ferrand, France
[b] Institute of Geochemistry and Petrology, ETH Zürich, Zürich, Switzerland
[c] Bayerisches Geoinstitut, Universität Bayreuth, 95447 Bayreuth, Germany
[d] GeoSoilEnvironmentCARS, Advanced Photon Source and the University of Chicago, Chicago, IL, United States

ARTICLE INFO

ABSTRACT

We have determined the valence state of Ytterbium (Yb) in a collection of meteorites covering 4–5 orders of magnitude in oxygen fugacity (fO_2) by X-ray absorption near-edge structure (XANES) spectroscopy at the Yb L2 edge. In the studied meteorite minerals, Yb abundance was between 1 and 30 ppm. The data were obtained from merrillite grains (theoretical formula $Ca_{18}Na_2Mg_2(PO_4)_{14}$) from two equilibrated ordinary chondrites (one H6 and one LL6), on oldhamite grains (theoretical formula CaS) from three EH enstatite chondrites (from EH3 to EH5) and four EL enstatite chondrites (from EL3 to EL6), on one merrilite grain and one stanfieldite grain (theoretical formula $Ca_4(Mg,Fe,Mn)_5(PO_4)_6$) from a pallasite, on merrillite grains from a eucrite, and in a phosphorous-bearing phase from an ungrouped primitive achondrite (NWA 11119). The obtained Yb XANES spectra were compared to those measured in terrestrial apatites (containing 17–79 ppm Yb) and in synthetic materials (metallic Yb, YbS, Yb_2S_3, Yb_2O_3). In terrestrial apatites, as well as in ordinary chondrites, in the eucrite, in the pallasite, and in the ungrouped achondrite NWA 11119, Yb is present as Yb^{3+} only. In enstatite chondrites, about half of the Yb in CaS is in the Yb^{2+} form and the fraction of Yb^{2+} may be slightly higher in EH compared to EL. It appears that Yb redox state can be used to build a redox scale for the most reduced objects of the Solar System as shown by this slight difference between EH and EL. However, the absence of a strong difference in Yb redox state between EH and EL chondrites suggests that the observed difference in Yb abundance anomalies in oldhamites found between EH and EL is not due to oxygen fugacity prevailing during parent-body equilibration but rather to fractionation related to volatility.

1. Introduction

Rare-earth elements (REE, restricted here to the lanthanides) are commonly used for geochemical modeling purposes because, as trace elements, their equilibrium partitioning between phases does not depend on their concentrations (Henry's law).

At ground state, lanthanides occur as [Xe] $4f^n 6s^2$ (or [Xe] $4f^{n-1} 5d^1 6s^2$ in the case of La, Ce, and Gd), and all elements of the group have the same outer electron shell configuration. They only differ by their 4f (or 5d) filling. Therefore, chemical bonding of the REE with ligands is similar along the series from La to Lu. In Earth's processes, REE usually occurs as 3+ cations, whose radii decrease smoothly from La to Lu (the lanthanide contraction). As a consequence, REE abundance patterns in

minerals vary smoothly because REE incorporation is controlled only by size mismatch between cation radii and crystallographic sites, as modelled by Wood and Blundy (1997) for the pyroxene-basalt case. Sometimes, however, Eu is observed to stick out from the rest of the REE. This is commonly interpreted as attesting for the reduction to Eu^{2+}, which has a larger radius and better fits in plagioclase Na-Ca site. Therefore, for terrestrial rocks, the so-called Eu anomaly is explained by valence change and reduction to Eu^{2+}. This conclusion may be extended to extraterrestrial material, such as lunar rocks (Papike et al., 1996), eucrites (Pun and Papike, 1996), and other achondrites (Frossard et al., 2019). In terrestrial materials, anomalies in Ce can also be found, which are explained by Ce oxidation to Ce^{4+} (Elderfield, 1988). A recent discussion about the significance of REE abundance anomalies can be found

---

in Barrat et al. (2023). The potential of Eu and Ce to be used as redox sensors in silicate melts has been the subject of several experimental calibrations (e.g., Burnham et al., 2015; Smythe and Brenan, 2015).

In the case of Yb, no concentration anomalies have been reported so far in terrestrial rocks, although the presence of Yb^{2+} has been suggested in some mantle rocks (Albalat et al., 2012). In enstatite chondrite, however, positive Yb anomalies have been reported in calcium sulfide (oldhamite, CaS) of the unequilibrated EH group (Crozaz and Lundberg, 1995; Gannoun et al., 2011; Hammouda et al., 2022). These anomalies occur together with Eu anomalies and, in some cases with Sm anomalies (to a lesser extent, as observed in oldhamites of unequilibrated EH chondrites (Gannoun et al., 2011; Hammouda et al., 2022). By comparison with experimental data Ingrao et al. (2019) interpreted the Yb anomalies as being caused by the presence of reduced Yb^{2+}. However, because Eu and Yb are the two most volatile REE in nebular processes (Lodders and Fegley, 1993), Hammouda et al. (2022) proposed that the observed positive anomalies in unequilibrated EH chondrites are due to a complex interplay between volatility and valence state, in which the oldhamite grains record the condensation of a residual gas after earlier condensation of material having negative Eu and Yb anomalies.

The purpose of the present work is to provide the first documentation of the valence state of Yb in natural objects and, in particular, to sample the Yb redox state in rocks coming from different regions of the Solar System. The most reduced objects studied are enstatite chondrites (EC). Their equilibrium redox conditions have been estimated by Brett and Sato (1984) using electrochemical methods and by Larimer and Buseck (1974), using the Si content of the metallic phase. The former found values of the order of IW-3 (that is, 3 log units below IW, where IW represents the Iron-Wustite equilibrium), whereas the latter calculated values below IW-10. When discussing their results, Brett and Sato recognized that their measurements on EC may have been contaminated by ambient atmosphere during sample preparation. The highly reduced character of enstatite chondrites is further attested by the study of Cr valence state in one EL3 of McKeown et al. (2014) who found that almost all Cr of olivine was present as Cr^{2+}, suggesting equilibration at about IW-6. Cartier et al. (2014) compiled some literature values and gave values around IW-6 for EH and IW-3 for EL chondrites. Therefore, we conclude that EC were equilibrated at conditions below IW-3, although a precise value may not be available at present. Brett and Sato (1984) also determined the oxygen fugacity of a pallasite (ca. IW-3), and of ordinary chondrites (ca. IW-1), two meteorite groups that are part of the present database. Although we did not study the same specimen as Brett and Sato did, we consider that their estimated values give a range of equilibrium conditions that are applicable to our case. Finally, we also studied a eucrite (NWA 15965) and the ungrouped achondrite NWA 11119, which formation conditions may be around IW-4 (Srinivasan et al., 2018). The dataset is completed by terrestrial apatites, which is an important repository for the REE for terrestrial samples.

2. Methods

2.1. X-ray absorption near-edge structure spectroscopy

The ytterbium valence state was determined by X-Ray Absorption Near Edge Structure (XANES) spectroscopy at the Yb L2 edge on 13-ID-E station of sector 13 (GSECARS) at the Advanced Photon Source. Both the L3 and the L2 edges were tested on an oldhamite crystal from enstatite chondrite. Previous work had shown that the L3 edge was fitted to study Yb valence state in experimental material, in which REE were doped to concentrations of the order of 100 ppm (Ingrao et al., 2019). In the case of the natural oldhamite, the spectra obtained at the L3 edge did not display a clear signal, which may be due to overlap with peaks from other REE or from transition metals that are present in the crystal. This point was not investigated further as the spectra at the L2 edge appeared suitable for studying Yb valence state.

Ytterbium L2-edge absorption spectra of a collection of samples of terrestrial and extraterrestrial origins were collected in fluorescence mode using a four-element, silicon-drift-diode detector array (Vortex-ME4, Hitachi High-Technologies Science America, Inc.) with pulse-processing provided by an Xspress 3 digital X-ray processor system (Quantum Detectors). All the fluorescence-mode XAFS data collected were corrected for detector dead time. Measurements of the samples were performed on optically-polished resin mounts, using a microbeam (ca. 2 x 3 μm) with an incident angle of 45 degrees. Given the low Yb concentrations involved (<80 ppm in the natural samples), self-absorption was considered negligible. Positioning on the sample surface was achieved using a dual optical microscope setup (Offline Sample Coordinate And Registration system), in which x – y coordinates were recorded outside the experimental station on a first microscope equipped with a motorized stage. The recorded coordinates were then transferred to a second microscope located inside the station, allowing for quick positioning. Both microscope optical axes were oriented normal to the surface sample, yielding excellent observation conditions for position checking and for focusing.

The energy was scanned between 9878 and 10,214 eV using the Si (111) crystal setup. The monochromator was calibrated using a Cu foil, which gave an E_0 (1st derivative of the edge) of 8980.44 eV for the K edge. Scan steps were 2.5 eV in the pre-edge region, 0.25 eV in the edge region. The post-edge region was scanned with a k-space step of 0.06 Å. Calibration of Yb absorption energy was achieved using commercial Yb metal foil (Goodfellow), YbS (NEYCO) for the divalent state and Yb_2S_3 (NEYCO) and Yb_2O_3 (Sigma Aldrich) for the trivalent state. Studying both sesquisulfide and sesquioxide allowed us to check whether the nature of the ligand would shift the position of the Yb^{3+} white line. All Yb compounds (oxide and sulfides) were studied as powder layers enclosed in tape, with no dilution. For YbS, the incident flux was decreased for analysis to reduce beam-induced speciation changes, which was observed in the specific case of this compound after repeated analysis on the same spot. Reference material data were acquired in transmission mode. Their edge-absorption energies were defined by the first maximum of the derivative in the spectra.

Raw data were processed using the Athena suite software (Ravel and Newville, 2005). The treatment included inspection of the individual spectra, correction, normalization, and merging. We also examined the variations of the derivative of the absorption relative to energy, which permits a more accurate estimation of the absorption edge, defined by the first maximum of the derivative. Finally, the software permits to decompose the absorption spectra in order to determine the contributions of the various ion valence states and coordinations to the total spectra.

For each studied sample, several grains of Yb-host phases were studied, when possible, that is depending on occurrence. In some cases, several analyses were performed in the same grain, to check for zoning.

3. Studied materials

We have selected materials that cover a range of Solar System objects (Earth, chondrites, achondrites) that were equilibrated under various redox conditions, from the most oxidized (Earth) to the most reduced (enstatite chondrites). For comparison with previous work, we also reinvestigated synthetic material that was previously analyzed at ESRF beamline BM23 (Ingrao et al., 2019). Although our collection does not reach the most oxidized objects of the Solar System (Cartier et al., 2014) its range is adapted to document Yb reduction. The selected materials are described in the following and their main features are summarized in Table 1. For most samples, information on REE concentrations were available. In some rare case, we did not have this information. This is not a problem, however, because here, we focus on Yb redox state and the shape of the XANES spectra does not depend on trace element concentration. (Self-absorption is negligible.)

For Earth's reference material, we used 3 different apatites. Apatite was chosen because this mineral can contain significant amounts of REE,

Table 1
Information on the materials studied for x-ray absorption at the Yb L2 edge.

	Class/type[a]	Host phase	Redox conditions[b]	Yb concentration (ppm)[c]	Nb of spectra[d]	Yb valence observed
Synthetic standards						
Yb°		Metal			1	Yb°
YbS		Sulfide			1	Yb^{2+}
Yb_2S_3		Sulfide			1	Yb^{3+}
Yb_2O_3		Oxide			1	Yb^{3+}
Experiments (Ingrao et al., 2019)						
#1250 (1300 °C)		CaS	IW-6.6 [1]	217 [1]	2	Yb^{2+} and Yb^{3+}
		Glass	IW-6.6 [1]	145 [1]	2	Yb^{2+} and Yb^{3+}
#1244 (1400 °C)		CaS	IW-5.8 [1]	98 [1]	2	Yb^{2+} and Yb^{3+}
		Glass	IW-5.8 [1]	407 [1]	2	Yb^{2+} and Yb^{3+}
Terrestrial material						
Apatite Durango		Apatite		29 [6]	1	Yb^{3+}
Apatite Hoggar		Apatite		79 [7]	1	Yb^{3+}
Apatite Xuxa		Apatite		17 [8]	1	Yb^{3+}
Ordinary chondrites						
Kernouvé	H6	Apatite	ca. IW-1 [2]	1 [9]	n.a.[e]	Yb^{3+}
		Merrillite	ca. IW-1 [2]	33 [9]	2	Yb^{3+}
Saint-Séverin	LL6	Apatite	ca. IW-1 [2]	3.5 [10]	n.a.[e]	Yb^{3+}
		Merrillite	ca. IW-1 [2]	30 [10]	2	Yb^{3+}
Enstatite chondrites						
Sahara 97158	EH3	Oldhamite	<IW-3 [2,3]	7 [11]	5	Yb^{2+} and Yb^{3+}
Abee	EH4-IMB	Oldhamite	<IW-3 [2,3]	10 [11]	0[f]	–
Oudiyat Sbaa	EH5	Oldhamite	<IW-3 [2,3]	11 [11]	10	Yb^{2+} and Yb^{3+}
Almahata Sitta, MS 189	EL3	Oldhamite	<IW-3 [2,3]	13 [11]	9	Yb^{2+} and Yb^{3+}
Almahata Sitta, MS 196	EL4/5	Oldhamite	<IW-3 [2,3]	13 [11]	2	Yb^{2+} and Yb^{3+}
Adrar Bous	EL5	Oldhamite	<IW-3 [2,3]	16 [11]	1	Yb^{2+} and Yb^{3+}
Hvittis	EL6	Oldhamite	<IW-3 [2,3]	14 [11]	10	Yb^{2+} and Yb^{3+}
Achondrites						
NWA 15965	Eucrite	Apatite	IW-1 [4]	n.d.	n.a.[e]	–
		Merrillite	IW-1 [4]	n.d.	4	Yb^{3+}
NWA 11119	Ungrouped	Phosphate	IW-4 [5]	n.d.	3	Yb^{3+}
Seymchan	Pallasite	Merrillite	IW-3 [2]	6–9 [12]	4	Yb^{3+}
		Stanfieldite	IW-3 [2]	1–3 [12]	4	Yb^{3+}

Notes:
[a] Refers to the meteorite class or the chondrite petrographic type.
[b] Sources for redox conditions: [1] Ingrao et al. (2019); [2] Brett and Sato (1984) data for chondrites and pallasite; [3] Larimer and Buseck (1974) for enstatite chondrites; [4] Wadhwa (2008); [5] Srinavasan et al. (2018).
[c] Sources for Yb concentrations: [1] Ingrao et al. (2019); [6] Émilie Bruand (pers. comm.); [7] Hammouda et al. (2010); [8] Santos Schuch (2018); [9] Heck et al. (2020); [10] this study; [11] Hammouda et al. (2022); [12] estimated from Chernonozhkin et al. (2021) data on Brahin and CMS 04071 pallasites (see main text); n.d., not determined.
[d] Number of spectra used for obtaining the merged spectra displayed in Figs. 1–9.
[e] Given the anticipated low Yb concentrations in apatites, these phases were not analyzed in ordinary chondrites and in the eucrite.
[f] For Abee, Yb concentration in oldhamite was too low to obtain acceptable spectra.

thus facilitating spectra acquisition. In addition, because in most of the extraterrestrial material studied, the REE were also hosted in phosphates, it seemed fitted to have a terrestrial phosphate for comparison. The only exception is the group of enstatite chondrites, in which calcium sulfide represents a major REE reservoir. In phosphate minerals, REE incorporation in the crystal lattice is controlled by various potential charge-balanced substitution mechanisms, in which the REE substitute for Ca, such as $Si^{4+} + REE^{3+} = Ca^{2+} + P^{5+}$, $2 REE^{3+} + vacancy = 3 Ca^{2+}$, $REE^{3+} + O^{2-} = Ca^{2+} + (OH, F, Cl)^-$, and $Na^+ + REE^{3+} = 2 Ca^{2+}$ (Fleet and Pan, 1995). In calcium sulfide, experimentally-obtained CaS/melt partition coefficient values display a relation with ionic radii of the REE (Ingrao et al., 2019). This also suggests crystal chemical control with the REE substituting for Ca, although the details of the substitution mechanism have not been explored.

The hydrothermal Durango apatite is a reference mineral for geochronology (Yang et al., 2014, Doucelance et al., 2020). Our specimen was provided by the National Museum of Natural History, Smithsonian Institution (sample #144954-4). Yang et al. (2014) compared different fragments analyzed by different groups and it appears that Durango apatite is slightly variable in composition. Its Yb content ranges between 27 and 59 ppm. Our fragment contains 29 ppm Yb (laser-ablation ICP-MS, E. Bruand, personal communication). The apatite from the carbonatitic complex of In Ouzzal (Ahaggar, Algeria) is similar to type III green apatite described in Ouzegane et al. (1988). It

has high levels of sulfur, SiO_2 and Sr and its LREE reach the oxide weight percent level. Its Yb concentration was determined by laser-ablation ICP-MS (Hammouda et al., 2010) and is 79 ppm. The Xuxa apatite from Brazil (Borborema, state of Paraíba) is found in skarns. It contains about 16 ppm Yb (Santos Schuch, 2018 by laser-ablation ICP-MS). It is currently being assessed as a reference material for geochronology (Santos Schuch, 2018, Antoine et al., 2020). Apatite having a hexagonal symmetry, it is possible that crystal orientation may affect the Yb absorption spectra. No such effect, however, was observed in the present investigation.

For the extraterrestrial material, we studied phosphates (merrillites, theoretical formula $Ca_{18}Na_2Mg_2(PO_4)_{14}$) from two ordinary chondrites (OC), Kernouvé (H6, Heck et al., 2020) and Saint-Séverin (LL6, this study). Phosphates in ordinary chondrites are usually considered of secondary, metamorphic origin (Zanda et al., 1994) with formation ages younger than that of the Solar System by a several My (e.g., ~4555 Myr for Saint-Séverin phosphates; Bouvier et al., 2007). Both chondrites contain apatite and merrillite. Apatites in both, however, have low Yb concentrations (between 1 and 3.5 ppm). Therefore, we focused on merrillites, which have Yb concentrations of 33 and 30 ppm in Kernouvé and Saint-Séverin, respectively.

Seven EC were studied, 3 EH (Sahara 97158 (EH3), Abee (EH4-IMB), Oudiyat Sbaa (EH5)) and 4 EL (MS 189 (EL3), MS 196 (EL4/5), Adrar Bous (EL5), Hvittis(EL6)). In EC, REE are mainly hosted by calcium

sulfide (CaS, oldhamite). Rare-earth element concentrations in the CaS of these 7 EC have been determined by Hammouda et al. (2022) using laser-ablation ICP-MS, and Yb concentrations in CaS range between 7 and 16 ppm. Because oldhamite has a cubic symmetry, no effect of crystallographic orientation on the Yb absorption spectra is expected. Typical oldhamite textures in EC have been presented in Hammouda et al. (2022). Additional scanning electron images are provided in Supplementary Material, with indication of XANES spots positions.

Three achondrites were studied. Seymchan is a pallasite. Our section contains two grains of phosphates: one merrillite and one stanfieldite (theoretical formula $Ca_4(Mg,Fe,Mn)_5(PO_4)_6$). Phosphates in pallasite are not primary phases. They have been interpreted as resulting from a reaction between melt and phosphoran olivine or by subsolidus reaction between metal and olivine (Davis and Olsen, 1991; Boesenberg et al., 2012). For the present study, we did not analyze our section for trace elements. By comparison with literature data (Hsu, 2003; Chernonozhkin et al., 2021), we infer Yb concentrations of the order of 6–9 ppm in merrillite, and of 1–3 ppm in stanfieldite. One eucrite (NWA 15965) contains merrillite and apatite grains and one ungrouped achondrite (NWA 11119) contains an unknown phosphorus-bearing phase. For the latter two samples, we do not have information on REE concentrations in the analyzed mineral phases.

4. Results

The recorded spectra are presented in Figs. 1–9. In the figure display, the energy range was restricted to between 9930 and 10,080 eV. Table 1 provides information of the number of spectra merged for the figure display. Table 1 also summarizes the observed valence states of Yb. Additional data, including individual spectra used for the merges and some enstatite chondrite samples listed in Table 1 but not presented in the figures are provided in the Supplementary Material.
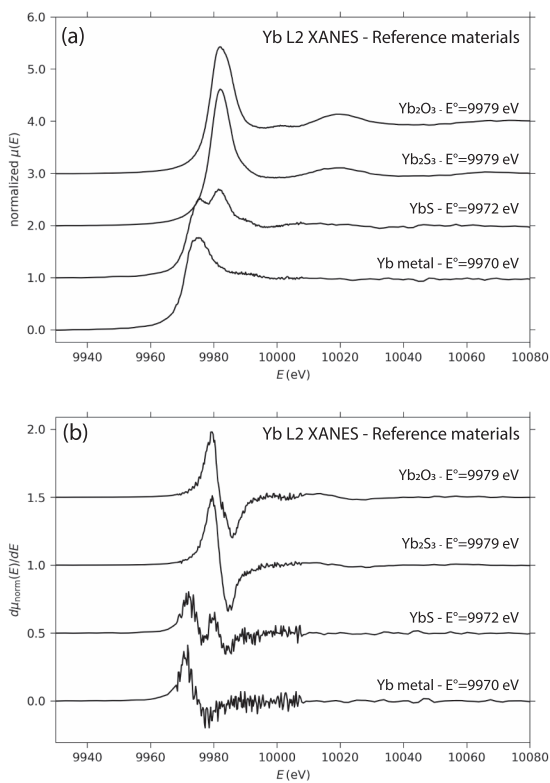
Fig. 1. X-ray absorption spectra at Yb L2 edge for reference materials: metallic Yb, YbS, Yb2S3, and Yb2O3. (a) Normalized absorptions. Absorption edge energy values are given for each compound. (b) Derivative of the absorption. The spectra are offset for clarity.
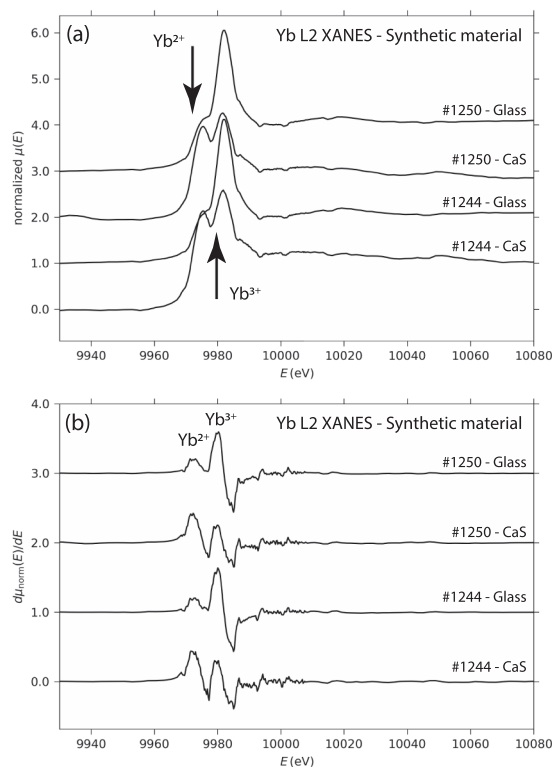
Fig. 2. X-ray absorption spectra at Yb L2 edge in glasses and calcium sulfides (CaS, oldhamite) for selected experiments published by Ingrao et al. (2019). (a) Normalized absorptions. (b) Derivative of the absorption. Each spectrum displayed results from merging 2 spectra recorded in 2 different spots in each phase. The spectra are offset for clarity. Note that Ingrao et al. (2019) used the Yb L3 absorption edge.

4.1. Reference compounds

XANES spectra for metallic Yb, YbS, Yb_2S_3, and Yb_2O_3 are displayed on Fig. 1. Metallic Yb exhibits an absorption peak at 9970 eV. YbS, in which Yb is theoretically divalent, displays a first peak at 9972 eV, followed by a second peak at 9979 eV. Finally, both Yb_2S_3, and Yb_2O_3 have a single absorption peak at 9979 eV, indicating that the nature of the ligand (whether it is sulfur or oxygen) does not affect the Yb absorption energy. Post-peak spectra of the two compounds differ, however. Although both have an oscillation at 10,020 eV, the oxide has an additional oscillation at 10,000 eV. Contrary to V (Wong et al., 1984) Nb and Ta (Cartier et al., 2015), there is no linear relation between Yb valence state and the energy of the absorption edge. In addition, the absorption edge of metallic Yb is very close to that of Yb^{2+} in YbS. Previous works on metallic Yb (Fuse et al., 2004; Dallera et al., 2006) have shown that the X-ray absorption edge of metallic Yb corresponds to a 2+ valence state at ambient conditions with a transition to the 3+ state at high pressure. A structural transformation, which was also attributed to the Yb^{2+} to Yb^{3+} transition, has been observed in Yb metal crystals by Hall et al. (1963) at 4 GPa with a change from face-centered cubic to body-centered cubic. Although these observations show that the notion of valence state as understood by material scientists may differ from that of mineralogists, further discussion on this topic is beyond the scope of the present paper.

4.2. Synthetic, experimental samples

X-ray absorption spectra of Yb in selected experiments published by Ingrao et al. (2019) are shown on Fig. 2. Here, we used the L2-edge, whereas Ingrao et al. (2019) studied the L3-edge on BM23 beamline of ESRF. The present data confirm the presence of both Yb^{2+} and Yb^{3+} with
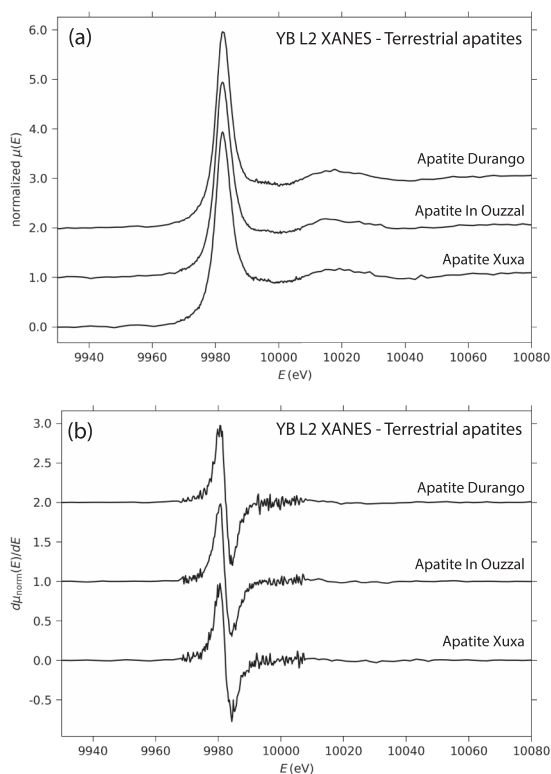
Fig. 3. X-ray absorption spectra at Yb L2 edge of 3 terrestrial apatites (Durango, In Ouzzal, Xuxa) containing varying amounts of Yb (see Table 1). (a) Normalized absorptions. (b) Derivative of the absorption. The spectra are offset for clarity.

Fig. 4. X-ray absorption spectra at Yb L2 edge in merrillites from 2 ordinary chondrites (Kernouvé, H6 and Saint-Séverin, LL6). (a) Normalized absorptions. (b) Derivative of the absorption. Each spectrum displayed result from merging 2 spectra recorded in 2 different merrillite grains in each chondrite. The data for Durango apatite is shown for comparison. The spectra are offset for clarity.

a preference of Yb^{2+} for the crystalline CaS relative to the melt. These results will not be further discussed in the following.

4.3. Natural terrestrial apatites

X-ray absorption spectra of Yb in terrestrial apatites are displayed in Fig. 3. All three apatites display a sharp absorption peak at 9979 eV, attesting for the presence of Yb^{3+} only. The chemical differences between the three apatite samples appear to have no effect on the post-peak region.

4.4. Ordinary chondrite phosphates

X-ray absorption spectra of Yb in merrillites from Kernouvé and from Saint-Séverin are shown in Fig. 4. All merrillite grains display a single peak at 9979 eV, corresponding to Yb^{3+}. Compared to terrestrial apatite, the position of the absorption edge is identical. Moreover, the post-edge oscillations of ordinary chondrite spectra are identical to those of terrestrial apatites, attesting for a similar crystallographic environment (nature of neighbors, coordination number and bond length), which is not much surprising given that the REE substitute for Ca in both phosphates, despite the difference in crystal structure between apatite and merrillite.

4.5. Enstatite chondrites oldhamites

X-ray absorption spectra of Yb in the studied oldhamites are shown in Fig. 5 for the EH chondrites and Fig. 6 for the EL chondrites. All spectra have a first edge at 9972 eV, followed by a second peak at 9979 eV. This attests for the presence of both Yb^{2+} and Yb^{3+} in all enstatite chondrites. Given the low Yb concentration, it is difficult to assess whether differences exist between the various enstatite chondrites. At first view, they

seem identical, suggesting that all enstatite chondrites have the same Yb^{2+}/Yb^{3+} ratio. This point will be further addressed later.
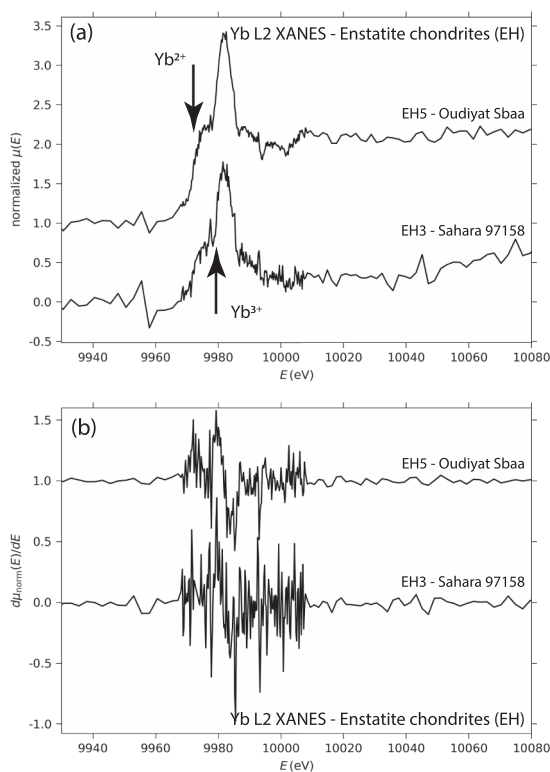
4.6. Achondrites

X-ray absorption spectra of Yb in merrillite and stanfieldite from the pallasite Seymchan are shown in Fig. 7. In both cases, only Yb^{3+} is present. Because of the very low Yb concentration (about 1–3 ppm as discussed above) the spectra obtained in the stanfieldite grain are noisy but their interpretation is straightforward.

X-ray absorption spectra of Yb in merrillites from eucrite NWA 15965 are shown in Fig. 8. Apatites were not studied, due to the anticipated low concentration of Yb by comparison with ordinary chondrites where merrillite and apatite are present together (see Table 1). In the studied eucrite, Yb is present in the form of Yb^{3+} in the merrillite grains and the post-peak oscillations are similar to those of the terrestrial apatites.

X-ray absorption spectra of Yb in the phosphorus-bearing phase of the ungrouped achondrite NWA 11119 are shown in Fig. 9. Here too, Yb appears to be mainly in the Yb^{3+} form. The post-peak oscillations are more difficult to discuss, which we attribute to a lower Yb concentration in the analyzed grains. If true, the main oscillation is compatible with a phosphate phase as the host for Yb.

5. Discussion

The redox state of the Solar System objects is important because, as an intensive parameter, it controls equilibrium phase relation, element behavior and distribution between coexisting phases during the accretion of planetary materials and planet growth. The material of choice in such endeavor is the direct study of meteorites, among which

Fig. 5. X-ray absorption spectra at Yb L2 edge in oldhamites of 2 EH chondrites (Sahara 97158, EH3 and Oudiyat Sbaa, EH5). (a) Normalized absorptions. (b) Derivative of the absorption. The spectra displayed result from merging 5 and 10 oldhamite spectra recorded in Sahara 97158 and Oudiyat Sbaa, respectively. Despite the noisy signal due to low Yb concentrations (between 7 and 11 ppm), both spectra show that the 2 EH oldhamites contain Yb2+ and Yb3+. The spectra are offset for clarity.
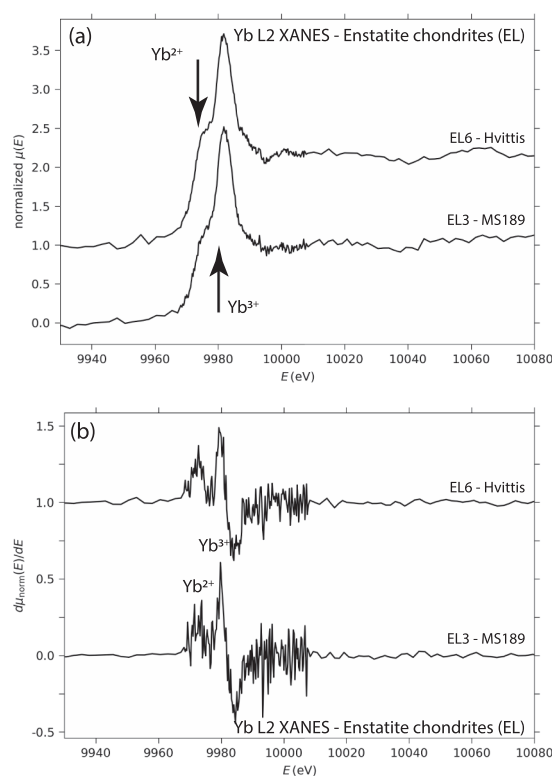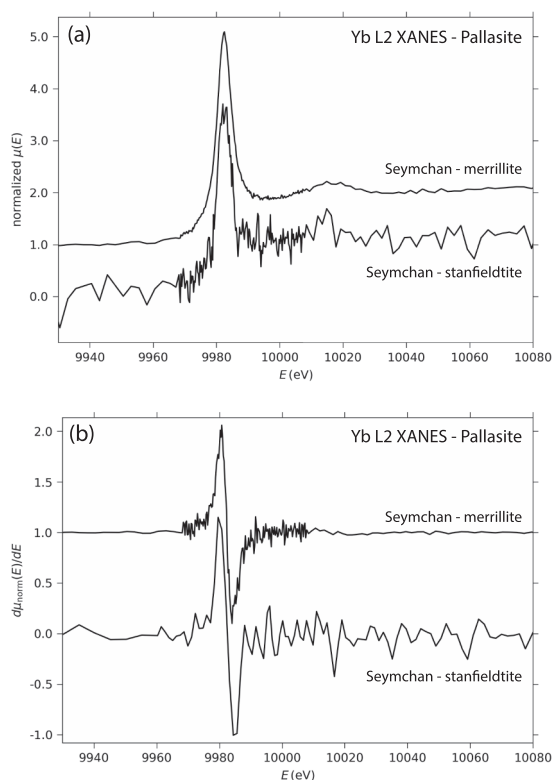

Fig. 6. X-ray absorption spectra at Yb L2 edge in oldhamites of 2 EL chondrites (MS189, EL3 and Hvittis, EL6). (a) Normalized absorptions. (b) Derivative of the absorption. The spectra displayed result from merging 9 and 10 oldhamite spectra recorded in MS189 and Hvittis, respectively. Note the presence of both Yb2+ and Yb3+. The spectra are offset for clarity.

chondrites, primitive achondrites, and iron meteorites represent fossils of the early stages of the Solar System evolution.

Various methods have been used to decipher the equilibrium redox conditions of meteorites. Phase equilibria between the metallic and the silicate phases have been used by Williams (1971), Larimer and Buseck (1974), among others. Metal – phosphate equilibria have also been considered (Olsen and Fuchs, 1967). Brett and Sato (1984) determined the intrinsic oxygen fugacity of a collection of meteorites (carbonaceous, ordinary, and enstatite chondrites and one pallasite) using an electrochemical cell. Another approach consists of studying the fractionation of elements with variable valence states, such as the transition elements (Cr, Fe, Ti, V) whose partitioning is sensitive to ambient redox conditions (Papike et al., 2004, 2005; Cartier et al., 2014, among others). Summaries of present knowledge of the oxidation state of various objects of the Solar System can be found in Wadhwa (2008) and Cartier et al. (2014).

5.1. Relation between host phase and Yb redox state

The Yb host phases studied here in extraterrestrial rocks can be divided into two categories: phosphates and sulfides. Phosphates host Yb (as well as other REE) in ordinary chondrites, in eucrites, in pallasite, as well as in other achondrites (except for aubrites, the enstatite achondrites, not studied here). In these meteorites, phosphates do not only host phosphorus, but they also carry halogens (F, Cl), in addition to hydrogen (in the form of (OH) groups). Therefore, they are important accessory minerals, as in terrestrial rocks.

Here, we found that the Yb XANES spectra of all investigated merrillites and stanfieldite grains are similar to those of terrestrial apatites, including the extended spectra. This is expected given that REE

substitute for Ca in phosphates and that Ca crystallographic sites are similar in all the investigated phosphate phases. In all investigated merrillites and stanfieldite grains, Yb appears to exist only in the trivalent state, Yb^{3+}.

In enstatite chondrite, a major host phase for the REE is oldhamite. In the specific case of Sahara 97158, which is a primitive EH chondrite, Hammouda et al. (2022) found that more than 80 % of the Yb budget was controlled by oldhamite. Because all enstatite chondrites have about the same amount of oldhamite (ca. 1 %) and all oldhamites have about the same Yb concentrations (Hammouda et al., 2022), it can be safely assumed that the Yb^{2+}/Yb^{3+} of oldhamite is a good proxy for that of the whole rock. In addition, because Yb (as the other REE) substitutes for Ca and because there is only one crystallographic site involved in the substitution, it can be safely assumed that the oldhamite Yb^{2+}/Yb^{3+} is solely controlled by the ambient oxygen fugacity, contrary to the case of Ti in hibonite, for which site preference has been shown to occur for Ti^{3+} and Ti^{4+} (Berry et al., 2017). Using the Athena software routine, we found that about 50 % of Yb^{2+} is present in this mineral. Yb^{2+} fraction was estimated by decomposing the Yb L2 edge absorption spectra using YbS and Yb_2S_3 as components and using the fraction of YbS contribution as a proxy for Yb^{2+}. The results are displayed in Fig. 10. The presence of oldhamite in enstatite chondrite is evidence for the highly reducing environment prevailing during their formation. In such conditions, refractory lithophiles elements, such as Ca, the lanthanides, the actinides become chalchophile (Lodders and Fegley, 1993; Gannoun et al., 2011). Here, we see that the change in REE chemical affinity is accompanied by reduction of the valence state of Yb.

5.2. Distribution of redox conditions in the early Solar System

Our results on Yb valence state on ordinary chondrites, and all the

Fig. 7. X-ray absorption spectra at Yb L2 edge in merrillite and stanfieldite from the pallasite Seymchan. (a) Normalized absorptions. (b) Derivative of the absorption. The spectra displayed result from merging 4 spectra recorded in a single grain of each phase. Due to the very low Yb concentration (estimated to 1–3 ppm), the spectrum of stanfieldite has been smoothed to remove the noise. The spectra are offset for clarity.

Fig. 8. X-ray absorption spectra at Yb L2 edge in merrillites from eucrite NWA 15965. (a) Normalized absorptions. (b) Derivative of the absorption. The spectrum displayed has been obtained by merging 4 spectra recorded in 4 different merrilite grains.

studied achondrites, with only Yb^{3+} present confirms that these meteorites are less reduced than enstatite chondrites. Brett and Sato (1984) report values of between IW-0.5 and IW-1.5 for ordinary chondrites and of about IW-3 for pallasites.

In the case of the pallasite Seymchan, phosphate grains are the host phase for the REE. The presence of phosphates (such as apatite, merrillite, stanfieldite, as reported in the present study, or other phases not studied here) in equilibrium with phosphides (schreibersite, $(Fe,Ni)_3P$ or $(Ni,Fe)_8(Si,P)_3$, among others) or Fe alloys containing phosphorus in solution has been used by Olsen and Fuchs (1967) to compute the oxygen fugacity of iron meteorites. The obtained values range between IW-2 and IW-3, in agreement with Brett and Sato (1984) results. This moderately reduced value fits well with the absence of Yb^{2+} in Seymchan.

In the case of the eucrite we have no evidence of a highly reduced parent body. On the basis of Si isotope measurements, Pringle et al. (2013) suggested that core segregation took place at redox condition of IW-4 on 4-Vesta, the proposed parent body of howardite-eucrite-diogenite (HED) meteorites. Righter and Drake (1997) and more recently Sikdar and Rai (2020) proposed that the HED parent body formed in the same region as that of ordinary and carbonaceous chondrites, at moderately reducing conditions around IW-2. Our results on Yb valence state cannot help in discriminating between the two oxygen fugacity values (see below for NWA 11119) but for later discussion, we will keep the IW-2 value, which appears to be more reasonable for the HED parent body.
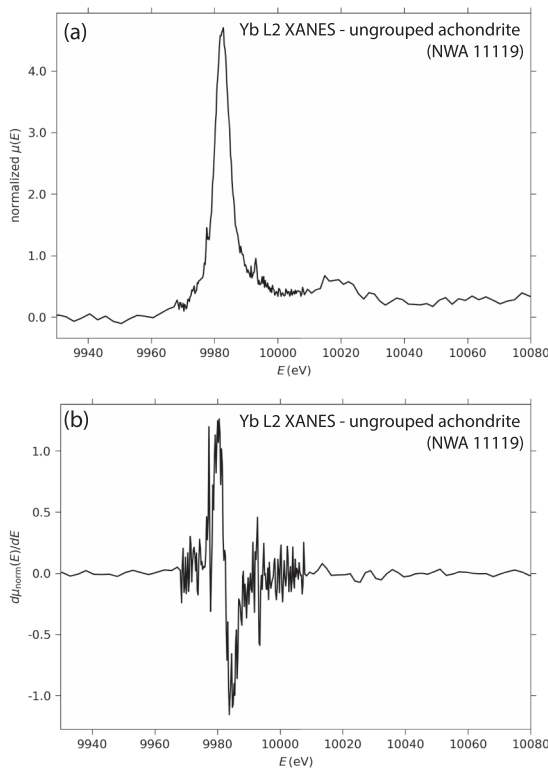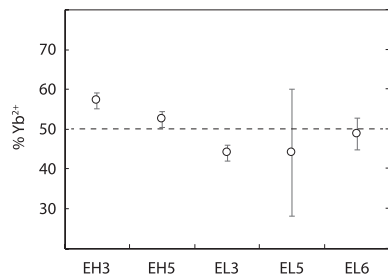
For the ungrouped achondrite NWA 11119 we also find no evidence of Yb^{2+}. Srinivasan et al. (2018) proposed that NWA 11119 was formed by melting of a precursor body of chondritic composition at conditions of the order of IW-4. The present data suggest that, even at IW-4, Yb
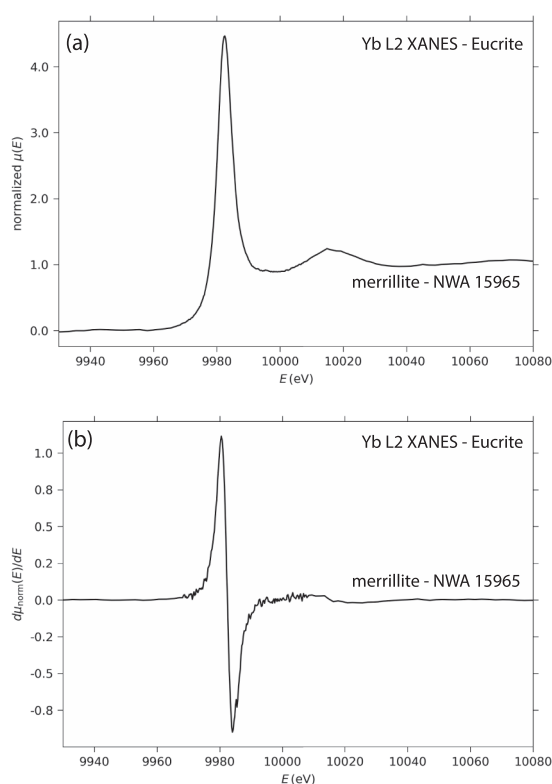
remains in the trivalent state. Thus, because all enstatite chondrites appear to be more reduced than NWA 11119 on the basis of their Yb^{2+}/Yb^{3+} ratio, the value of IW-4 must represent an upper bound for fO_2 equilibrium conditions of enstatite chondrites.

Our Yb data confirm the highly reduced conditions of the enstatite chondrites. Earlier oxygen fugacity of EC estimation by Brett and Sato (1984) is about IW-3, a value the authors considered as being an upper limit, due to potential contamination by the laboratory atmosphere. Larimer and Buseck (1974) have obtained values of EC oxygen fugacity using the Si content of the metal. They give values below IW-11, which is highly reducing. When plotted on a ΔIW vs reciprocal temperature diagram, Larimer and Buseck (1974) results may suggest that EH could be more reduced than EL because the two data subsets are offset by about 0.5 log unit (Fig. 11). Our results on Yb^{2+}/Yb^{3+} ratios shown in Fig. 10 may confirm this difference but both our data and those of Larimer and Buseck (1974) have significant uncertainties. As shown in Fig. 11, EH and El data points can be collapsed to a single line if a 25 K value is added or removed to either data subset. This 25 K values is largely within the uncertainty of thermodynamic modeling. Similarly, our data on Yb valence state have significant error bars and it is not so clear as to whether the observed difference between EH and EL is real. Cartier et al. (2014) compiled literature data and have suggested values of the order of IW-6 for EH and IW-3 for EL. In light of the present results on Yb valence state, the EL value should be lowered in order to match that of EH. Lastly, it is remarkable that all analyzed CaS have similar Yb XANES spectrum, although their REE abundance patterns vary widely among enstatite chondrites as recently documented, with EH3 having concave upward CI-normalized REE patterns with positive Eu and Yb anomalies, EH5 having flat patterns, and EL having convex upward CI-normalized REE patterns with a Eu negative anomaly and no Yb anomaly (Hammouda et al., 2022). Therefore, whatever the complex processes that yielded such a variety of patterns, they must have yielded only a slight, if
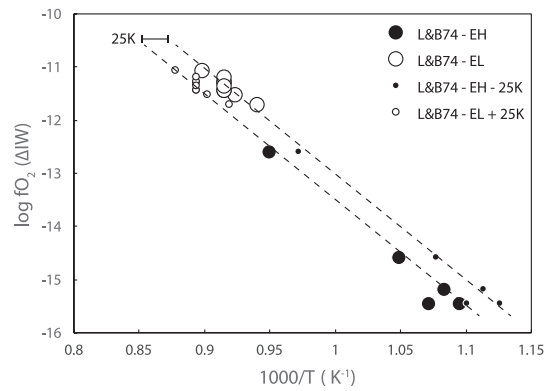
Fig. 9. X-ray absorption spectra at Yb L2 edge in the phosphorus-bearing phase in the ungrouped achondrite NWA 11119. (a) Normalized absorptions. (b) Derivative of the absorption. The spectrum displayed has been obtained by merging 3 spectra recorded in 3 different grains.
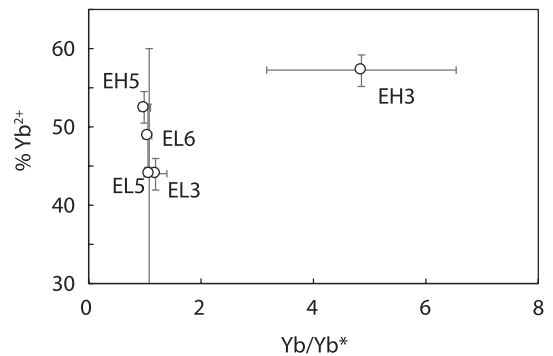

Fig. 11. Calculated oxygen fugacity vs. reciprocal temperature for enstatite chondrites, using the scheme of Larimer and Buseck (1974) based on Si concentration in metal. The temperatures were determined together with oxygen and sulfur fugacities by combining the three following equilibria. $Si + O_2 = SiO_2$; $2 CaSiO_3 + S_2 = 2 CaS + 2 SIO_2 + O_2$; $2 Fe + S_2 = 2 FeS$. Large filled and empty circles represent EH and EL data, respectively, using the temperature estimates given by Larimer and Buseck (1974). The small filled and empty circles represent recalculated EH and EL data, respectively, with modified temperatures (-25 K for EH or $+25$ K for EL). Note that the offset between EH and EL is no longer present if equilibrium temperatures are modified. Given the overall uncertainties in the modeling, it is therefore not clear whether the redox difference between EH and EL is real. See text for further discussion.


Fig. 10. Fraction of Yb^{2+} relative to total Yb in oldhamites of the studied enstatite chondrites. Yb^{2+}fraction was estimated using the fraction of YbS relative to [YbS + Yb2S3] in decomposed Yb L2 absorption edge spectra as a proxy. Error bars on Yb^{2+} fractions are obtained from Athena data reduction suite. The presence of only 1 available spectrum for EL5 is the cause for the large error bar. All other spectra treated were merges of several spectra as discussed in the main text and noted in the captions of Figs. 5 and 6.

Fig. 12. Fraction of Yb^{2+} relative to total Yb in oldhamites of the studied enstatite chondrites expressed as a function of Yb anomaly Yb*/Yb, with Yb* being the value of Yb concentration interpolated between Lu and Tm (or Er), and Yb that was actually measured in the samples. No salient relation between Yb^{2+} and Yb/Yb* is observed. All concentration values are taken from Hammouda et al. (2022).

any, change in oxygen fugacity between EH and EL. This conclusion is further substantiated by the absence of any clear relation between Yb^{2+} abundance and Yb concentration anomalies in enstatite chondrites, as illustrated in Fig. 12.

The relation of Yb^{2+} fraction vs. intrinsic meteorite oxygen fugacity is summarized in Fig. 13. This diagram attempts to document Yb valence change in Solar System objects, as a function of oxygen fugacity. In this diagram, the position of the enstatite chondrites is somehow arbitrary given the difficulty to obtain a reliable value for their fO₂. The present Yb valence-state data suggest that enstatite chondrite redox state should be below IW-4.

6. Conclusion

Although Yb^{2+} appears to be restricted to the most reduced objects of the Solar System, the ytterbium valence state could be used to discriminate meteorite parent body redox state on the low end of the oxygen fugacity range. Synchrotron-based X-ray absorption near-edge spectroscopy is a powerful tool to investigate the redox state of seldom-considered elements, given their high dilution in minerals (ppm level). It is remarkable that highly reduced states can be preserved in the meteorite record, not only for observed falls but also for finds, such as the Sahara samples. Our approach may open new ways of studying the redox state of the Solar System materials.

Recently, Hammouda et al. (2022) proposed a complex, multistage scenario involving fractional condensation, high-temperature events including partial vaporization and melting at a very early stage of the Solar System to explain the diversity of REE patterns of oldhamites in enstatite chondrites. A complex history involving partial evaporation followed by recondensation was also proposed for refractory calcium-,
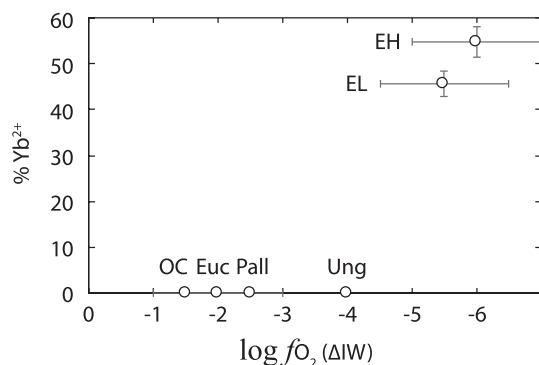
Fig. 13. Tentative Yb^{2+} fraction vs. oxygen fugacity (expressed relative to IW equilibrium) diagram for the studied meteorites. The values of Yb^{2+} fraction for enstatite chondrite has been averaged from the values presented in Fig. 10. Values for fO_2 of ordinary chondrites, the eucrite, the pallasite, and the ungrouped NWA 111119 are taken the literature (see discussion in the main text). For enstatite chondrites, EH and EL have been assigned values of IW-6 and IW-5.5, respectively. These values are somehow arbitrary, but note that the actual value for these groups may be lower (Larimer and Buseck, 1974). Other abbreviations are: OC = ordinary chondrites; Euc = eucrite; Pall = pallasite, Ung = ungrouped achondrite NWA 11119.

aluminum-rich inclusions (CAI) of Allende CV chondrite by Hu et al. (2021) using REE stable isotope fractionations. In the case of enstatite chondrites, whatever the details of the thermal history, the present Yb redox state data suggest that CaS evolution has taken place under rather constant redox conditions, despite the loss of a fraction of iron and sulfur from the EL parent body relative to that of EH. Whether this oxygen-fugacity buffering was internally or externally imposed on the parent body (closed vs. open system) is yet to be discussed when modeling small planetesimal-collision processes.

Data availability

Data are available through the OPGC catalog at https://doi.org/10.25519/JFCN-B685.

CRediT authorship contribution statement

Tahar Hammouda: Writing – review & editing, Writing – original draft, Project administration, Investigation, Funding acquisition, Formal analysis, Conceptualization. **Paul Frossard:** Writing – review & editing, Writing – original draft, Investigation, Formal analysis. **Maud Boyet:** Writing – review & editing, Writing – original draft, Investigation, Funding acquisition. **Audrey Bouvier:** Writing – review & editing, Writing – original draft. **Matthew Newville:** Methodology, Investigation. **Antonio Lanzirotti:** Writing – review & editing, Methodology, Investigation.

Declaration of competing interest

The authors declare that they have no known competing financial interests or personal relationships that could have appeared to influence the work reported in this paper.

Appendix A. Supplementary material

A supplementary file is attached to this article. This file is divided in 3 sections. S1 presents scanning electron images of oldhamite grains from a selection of enstatite chondrites, in which the positions of the areas analyzed by XANES are indicated. S2 presents the individual Yb L2-edge absorption edge spectra of the analyzed meteorites, whose averages are displayed in the figures of the main text. S3 presents fits of the reference materials (YbS and Yb_2S_3) to the oldhamite spectra recorded in enstatite chondrites. Supplementary material to this article can be found online at https://doi.org/10.1016/j.gca.2024.03.018.

References

Albalat, E., Telouk, P., Albarède, F., 2012. Er and Yb isotope fractionation in planetary materials. Earth Planet Sci. Lett. 355–356, 39–50.

Antoine, C., Bruand, E., Guitreau, M., Devidal, J.-L., 2020. Understanding preservation of primary signatures in apatite by comparing matrix and zircon-hosted crystals from the Eoarchean Acasta Gneiss Complex (Canada). Geochem. Geophys. Geosyst. 21, e2020GC008923.

Barrat, J.-A., Bayon, G., Lalonde, S., 2023. Calculation of cerium and lanthanum anomalies in geological and environmental samples. Chem. Geol. 615, 121202.

Berry, A.J., Schofield, P.F., Kravtsova, A.N., Miller, L.A., Stephen, N.R., Walker, A.M., Soldatov, A.V., Ireland, T.R., Geraki, K., Mosselmans, J.F.W., 2017. The limitations of hibonite as a single-mineral oxybarometer for early solar system processes. Chem. Geol. 466, 32–40.

Boesenberg, J.S., Delaney, J.S., Hewins, R.H., 2012. A petrological and chemical reexamination of Main Group pallasite formation. Geochim. Cosmochim. Acta 89, 134–158.

Bouvier, A., Blichert-Toft, J., Moynier, F., Vervoort, J.D., Albarède, F., 2007. Pb–Pb dating constraints on the accretion and cooling history of chondrites. Geochim. Cosmochim. Acta 71, 1583–1604.

Brett, R., Sato, M., 1984. Intrinsic oxygen fugacity measurements on seven chondrites, a pallasite, and a tektite and the redox state of meteorite parent bodies. Geochim. Cosmochim. Acta 48, 111–120.

Burnham, A.D., Berry, A.J., Halse, H.R., Schofield, P.F., Cibin, G., Mosselmans, J.F.W., 2015. The oxidation state of europium in silicate melts as a function of oxygen fugacity, composition and temperature. Chem. Geol. 411, 248–259.

Cartier, C., Hammouda, T., Doucelance, R., Boyet, M., Devidal, J.-L., Moine, M., 2014. Experimental study of trace element partitioning between enstatite and melt in enstatite chondrites at low oxygen fugacities and 5 GPa. Geochim. Cosmochim. Acta 130, 167–187.

Cartier, C., Hammouda, T., Boyet, M., Mathon, O., Testemale, D., Moine, B.N., 2015. Evidence for Nb^{2+} and Ta^{3+} in silicate melts under highly reducing conditions: a XANES study. Am. Mineral. 100, 2152–2158.

Chernonozhkin, S.M., McKibbin, S.J., Goderis, S., Van Malderen, S.J.M., Claeys, P., Vanhaecke, F., 2021. New constraints on the formation of main group pallasites derived from in situ trace element analysis and 2D mapping of olivine and phosphate. Chem. Geol. 562, 119996.

Crozaz, G., Lundberg, L.L., 1995. The origin of oldhamite in unequilibrated enstatite chondrites. Geochim. Cosmochim. Acta 59, 3817–3831.

Dallera, C., Wessely, O., Colarieti-Tosti, M., Eriksson, O., Ahuja, R., Johansson, B., Katsnelson, M.I., Annese, E., Rueff, J.-P., Vankó, G., Braicovich, L., Grioni, M., 2006. Understanding mixed valent materials: Effects of dynamical core-hole screening in high-pressure x-ray spectroscopy. Phys. Rev. B 74, 081101(R).

Davis, A.M., Olsen, E.J., 1991. Phosphates in pallasite meteorites as probes of mantle processes in small planetary bodies. Nature 353, 637–640.

Doucelance, R., Bruand, E., Matte, S., Bosq, C., Auclair, D., Gannoun, A., 2020. In-situ determination of Nd isotope ratios in apatite by LA-MC-ICPMS: Challenges and limitations. Chem Geol 550, 119740.

Elderfield, H., 1988. The oceanic chemistry of the rare-earth elements. Philos. Trans. Roy. Soc. Lond. Ser. A 325, 105–126.

Fleet, M.E., Pan, Y., 1995. Site preference of rare earth elements in fluorapatite. Am. Mineral. 80, 329–335.

Frossard, P., Boyet, M., Bouvier, A., Hammouda, T., Monteux, J., 2019. Evidence for anorthositic crust formed on an inner solar system planetesimal. Geochem. Persp. Let. 11, 28–32.

Fuse, A., Nakamotoa, G., Kurisu, M., Ishimatsu, N., Tanida, H., 2004. The valence state of Yb metal under high pressure determined by XANES measurement up to 34.6 GPa. J. Alloys Comp. 376, 34–37.

Gannoun, A., Boyet, M., El Goresy, A., Devouard, B., 2011. REE and actinide microdistribution in Sahara 97072 and ALHA77295 EH3 chondrites: a combined cosmochemical and petrologic investigation. Geochim. Cosmochim. Acta 75, 3269–3289.

Hall, H.T., Barnett, J.D., Merrill, L., 1963. Ytterbium: transition at high pressure from face-centered cubic to body-centered cubic structure. Science 139, 111–112.

Hammouda, T., Chantel, J., Devidal, J.-L., 2010. Apatite solubility in carbonatitic liquids and trace element partitioning between apatite and carbonatite at high pressure. Geochim. Cosmochim. Acta 74, 7220–7235.

Hammouda, T., Boyet, M., Frossard, P., Cartier, C., 2022. The message of oldhamites from enstatite chondrites. Progr. Earth Planet. Sci. 9, 13.

Heck, P.R., et al., 2020. The fall, recovery, classification, and initial characterization of the Hamburg, Michigan H4 chondrite. Meteorit. Planet. Sci. 55, 2341–2359.

Hsu, W., 2003. Minor element zoning and trace element geochemistry of pallasites. Meteorit. Planet. Sci. 38, 1217–1241.

Hu, J.Y., Dauphas, N., Tissot, F.L.H., Yokochi, R., Ireland, T.J., Zhang, Z., Davis, A.M., Ciesla, F.J., Grossman, L., Charlier, B.L.A., Roskosz, M., Alp, E.E., Hu, M.Y., Zhao, J., 2021. Heating events in the nascent solar system recorded by rare earth element isotopic fractionation in refractory inclusions. Sci. Adv. 7, eaaC962.

Ingrao, N.J., Hammouda, T., Boyet, M., Gaborieau, M., Moine, B.N., Vlastelic, I., Bouhifd, M.A., Devidal, J.-L., Mathon, O., Testemale, D., Hazemann, J.-L., Proux, O., 2019. Rare earth element partitioning between sulphides and melt: evidence for Yb^{2+} and Sm^{2+} in EH chondrites. Geochim. Cosmochim. Acta 265, 182–197.

Larimer, J.W., Buseck, P.R., 1974. Equilibration temperatures in enstatite chondrites. Geochim. Cosmochim. Acta 38, 471–477.

Lodders, K., Fegley, B., 1993. Lanthanide and actinide chemistry at high C/O ratios in the solar nebula. Earth Planet Sci. Lett. 117, 125–145.

McKeown, D.A., Buechele, A.C., Tappero, R., McCoy, T.J., Gardner-Vandy, K.G., 2014. X-ray absorption characterization of Cr in forsterite within the MacAlpine Hills 88136 EL3 chondritic meteorite. Am. Mineral. 99, 190–197.

Olsen, E., Fuchs, L.H., 1967. The state of oxidation of some iron meteorites. Icarus 6, 242–253.

Ouzegane, K., Fourcade, S., Kienast, J.-R., Javoy, M., 1988. New carbonatite complexes in the Archean In'Ouzzal nucleus (Ahaggar, Algeria): mineralogical and geochemical data. J. Petrol. 98, 277–292.

Papike, J.J., Fowler, G.W., Shearer, C.K., Layne, G.D., 1996. Ion microprobe investigation of lagioclase and orthopyroxene from lunar Mg-suite norites: Implications for calculating parental melt REE concentrations and for assessing postcrystallization REE redistribution. Geochim. Cosmochim. Acta 60, 3967–3978.

Papike, J.J., Karner, J.M., Shearer, V.K., 2004. Comparative planetary mineralogy: V/(Cr + Al) systematics in chromite as an indicator of relative oxygen fugacity. Am. Mineral. 89, 1557–1560.

Papike, J.J., Karner, J.M., Shearer, V.K., 2005. Comparative planetary mineralogy: Valence state partitioning of Cr, Fe, Ti, and V among crystallographic sites in olivine, pyroxene, and spinel from planetary basalts. Am. Mineral. 90, 277–290.

Pringle, E.A., Savage, P.S., Badro, J., Barrat, J.-A., Moynier, F., 2013. Redox state during core formation on asteroid 4-Vesta. Earth Planet Sci. Lett. 373, 75–82.

Pun, A., Papike, J.J., 1996. Unequilibrated eucrites and the equilibrated Juvinas eucrite: Pyroxene REE systematics and major, minor, and trace element zonig. Am. Mineral. 81, 1438–1451.

Ravel, B., Newville, M., 2005. ATHENA, ARTEMIS, HEPHAESTUS: Data analysis for X-ray absorption spectroscopy using IFEFFIT. J. Synchr. Rad. 12, 537–541.

Righter, K., Drake, M.J., 1997. A magma ocean on Vesta: Core formation and petrogenesis of eucrites and diogenites. Meteorit. Planet. Sci. 32, 929–944.

Santos Schuch, C., 2018. Caracterização de apatitas da província Borborema, NE do Brasil, como materiais de refereência para geocronologia U-Pb via LA-ICP-MS. Trabalho de conclusão de curso, Universidade Federal de Ouro Preto, Escola de Minas, Departamento de Geologia, Monografia no 280, 91p.

Sikdar, J., Rai, V.K., 2020. Si-Mg isotopes in enstatite chondrites and accretion of reduced planetary bodies. Sci. Rep. 10, 1273.

Smythe, D.J., Brenan, J.M., 2015. Cerium oxidation state in silicate melts: Combined fO_2, temperature and compositional effects. Geochim. Cosmochim. Acta 170, 173–187.

Srinivasan, P., Dunlap, D.R., Agee, C.B., Wadhwa, M., Coleff, D., Ziegler, K., Zeigler, R., McCubbin, F.M., 2018. Silica-rich volcanism in the early solar system dated at 4.565 Ga. Nat. Comm. 9, 3036.

Wadhwa, M., 2008. Redox Conditions on Small Bodies, the Moon and Mars. Rev. Mineral. Geochem. 68, 493–510.

Williams, R.J., 1971. Equilibrium temperatures, pressures, and oxygen fugacities of the equilibrated chondrites. Geochim. Cosmochim. Acta 35, 407–411.

Wong, J., Lytle, F.W., Messmer, R.P., Maylotte, D.H., 1984. X-edge absorption spectra of selected vanadium compounds. Phys. Rev. B 30, 5596–5610.

Wood, B.J., Blundy, J.D., 1997. A predictive model for rare earth element partitioning between clinopyroxene and anhydrous silicate melt. Contrib. Miner. Petrol. 129, 166–181.

Yang, Y.H., Wu, F.Y., Yang, J.H., Chew, D.M., Xie, L.W., Chu, Z.Y., Zhang, Y.B., Huang, C., 2014. Sr and Nd isotopic compositions of apatite reference materials used in U-Th–Pb geochronology. Chem. Geol. 385, 35–55.

Zanda, B., Bourot-Denise, M., Perron, C., Hewins, R.H., 1994. Origin and metamorphic redistribution of silicon, chromium, and phosphorus in the metal of chondrites. Science 265, 1846–1849.